

# Maskless Projection Lithography for the Fast and Flexible Generation of Grayscale Protein Patterns

Ansgar Waldbaur, Björn Waterkotte, Katja Schmitz, and Bastian E. Rapp\*

*Protein patterns of different shapes and densities are useful tools for studies of cell behavior and to create biomaterials that induce specific cellular responses. Up to now the dominant techniques for creating protein patterns are mostly based on serial writing processes or require templates such as photomasks or elastomer stamps. Only a few of these techniques permit the creation of grayscale patterns. Herein, the development of a lithography system using a digital mirror device which allows fast patterning of proteins by immobilizing fluorescently labeled molecules via photobleaching is reported. Grayscale patterns of biotin with pixel sizes in the range of 2.5  $\mu\text{m}$  are generated within 10 s of exposure on an area of about 5  $\text{mm}^2$ . This maskless projection lithography method permits the rapid and inexpensive generation of protein patterns definable by any user-defined grayscale digital image on substrate areas in the  $\text{mm}^2$  to  $\text{cm}^2$  range.*

## 1. Introduction

Protein patterns of different shapes and densities are of great interest for the investigation of molecular processes that control cellular behavior. They also play an important role in the design of biomaterials that exert control over the cells growing on them. If the sophisticated patterns and gradients formed by proteins on the cell surface and inside tissues can be reliably mimicked, the molecular parameters controlling cellular processes such as adhesion, migration, and differentiation can be identified. These insights will guide the development of functional biomaterials such as noninflammatory implants or

neural interfaces for artificial sensors. As individual cells may show different responses to a similar setup, large numbers of single-cell experiments need to be performed repeatedly under well-defined conditions to obtain results that can be generalized. Alternatively, large-scale protein patterns (on an area of several  $\text{mm}^2$  to  $\text{cm}^2$ ) would allow parallel assays and therefore an inherent increase in experimental throughput.

Thus, quick and easy techniques for the reproducible creation of spatially constrained protein patterns are required. A number of techniques for the generation of two-dimensional protein patterns have been presented and discussed in the literature. These techniques differ in processable lateral size, resolution, and processing time for the transfer of the basic pattern onto the substrate. Some techniques only allow the creation of binary patterns, whereas others allow the creation of “grayscale” patterns which are required to create protein density gradients. Several techniques allow patterning within a single process step (parallel patterning), whereas other techniques are serial in nature so that pattern generation times strongly depend on the complexity and size of the pattern to be created. An overview of important techniques and their characteristics is given in **Table 1**.

A straightforward method for the creation of binary patterns is direct spotting of protein solutions onto the substrate. To obtain patterns with small feature sizes the droplets deposited have to be as small as possible. Using capillaries of about 100 nm opening diameter and applying a voltage between the fluid to be deposited and the capillary, feature

A. Waldbaur, Dr. B. E. Rapp  
Institute of Microstructure Technology (IMT)  
KIT, Hermann-von-Helmholtz-Platz 1,  
76344 Eggenstein-Leopoldshafen, Germany  
E-mail: bastian.rapp@kit.edu

B. Waterkotte, Prof. K. Schmitz  
Institute of Organic Chemistry (IOC)  
KIT, Fritz-Haber-Weg 6,  
76131 Karlsruhe, Germany, and Institute of Functional Interfaces (IFG)  
KIT, Hermann-von-Helmholtz-Platz 1,  
76344 Eggenstein-Leopoldshafen, Germany

Prof. K. Schmitz  
Clemens-Schöpf-Institute of Organic Chemistry and Biochemistry  
Technical University of Darmstadt  
Petersenstraße 22, 64287 Darmstadt, Germany

DOI: 10.1002/sml.201102163



**Table 1.** Overview of 2D patterning techniques.

Technique	Direct/replicative	Pattern	Resolution <sup>a)</sup>	Transfer time <sup>b)</sup>	Serial/parallel	Ref.
<b>Mechanical</b>						
direct spotting	direct	binary	800 nm	10 s/spot	serial	[1]
dip-pen	direct	binary	55 nm	0.5 s/spot	serial	[3]
nanolithography (DPN)			0.6–1.0 $\mu\text{m}$	n.a.	parallel	[33]
microfluidic channel networks ( $\mu\text{FN}$ )	replicative	grayscale	$\approx 1 \mu\text{m}$	1 h/pattern	parallel	[9]
microcontact printing ( $\mu\text{CP}$ )	replicative	binary	150 nm	10 min/stamp	parallel	[34]
		grayscale	2 $\mu\text{m}$	2 min/stamp	parallel	[35]
<b>Photolithographic</b>						
resist based	replicative	binary	1–2 $\mu\text{m}$	8–10 s	parallel	[36]
direct writing <sup>c)</sup>	direct	grayscale	100 nm	2.5 $\mu\text{m s}^{-1}$	serial	[37]
photodeprotection	replicative	binary	10–15 $\mu\text{m}$	10 min/pattern	parallel	[30]
	direct	binary	180 nm	1 $\mu\text{m s}^{-1}$	serial	[38]
	direct	grayscale	900 nm	2–402 s/field	serial	[15]
photoactivation	replicative	binary	0.7 $\mu\text{m}$	1 s	parallel	[18,39]
	direct	grayscale	70 $\mu\text{m}$	37–592 s/field	serial	[40]
<b>Photoactivated protein adsorption<sup>d)</sup></b>						
mask based	replicative	binary	7 $\mu\text{m}$	30 min/pattern	parallel	[25]
laser writing (LAPAP)	direct	grayscale	1 $\mu\text{m}$	5–50 $\mu\text{m min s}^{-1}$	serial	[26]
spatial light modulator	replicative	grayscale	1.5 $\mu\text{m}$	30 min/pattern	parallel	[27]
digital mirror device	replicative	grayscale	2.5 $\mu\text{m}$	10 s/pattern	parallel	this paper

<sup>a)</sup>Width of smallest pattern element (spot diameter, line width, line spacing etc.); <sup>b)</sup>Time to generate functionalized pattern. The protein may be transferred directly or be immobilized to a pattern of functionalized linkers. Incubation steps prior to stamping or after pattern generation need to be added; <sup>c)</sup>Has not been reported for protein patterns yet; <sup>d)</sup>This is a special case of photolithography based on photoactivation.

sizes down to 5  $\mu\text{m}$  and less could be produced.<sup>[1]</sup> Finer structures can be achieved by transfer techniques based on scanning probe microscopy in which the cantilever tip is used to deposit biomolecules on a surface. If thiols are delivered to a gold surface to form self-assembled monolayers (SAMs), the term dip-pen nanolithography (DPN) is used.<sup>[2]</sup> If functionalized thiols are used as inks, small molecules as well as proteins and other biomolecules can be covalently linked to these patterns.<sup>[3]</sup> The smallest features of  $2 \times 4 \text{ nm}^2$  were obtained by an inked atomic force microscopy (AFM) tip scratching a SAM and filling the gap with the respective ink.<sup>[4]</sup> Direct writing techniques like spotting and DPN are serial patterning processes, therefore the processing time increases with increasing substrate size.

The most common technique for parallel patterning is the use of structured elastomers as stamp templates for contact printing, usually termed microcontact printing ( $\mu\text{CP}$ ).<sup>[5]</sup> This technique is used to print protein solutions onto planar surfaces by means of a stamp typically created in soft hydrophobic elastomers such as polydimethylsiloxane (PDMS). If the surface of the stamp is uniformly wetted with the ink, a complex pattern can be transferred onto a substrate within seconds.  $\mu\text{CP}$  has been demonstrated for features as small as several hundred nanometers.<sup>[6]</sup> The stamps can be reused so that large numbers of uniform patterns can be created for repetitive experiments. As stamping leads to binary patterns, gradients have to be simulated by

increasing line or spot densities.<sup>[7]</sup> Alternatively, one- and two-dimensional gradients have been created using elastomer stamps of variable thickness that deliver thiols to surfaces in densities corresponding to stamp thickness.<sup>[8]</sup> Linear gradients were also created by diffusion of proteins into flat agarose stamps and transferred directly onto functionalized surfaces.<sup>[7]</sup>

An alternative to  $\mu\text{CP}$  is the use of microfluidic channel networks ( $\mu\text{FN}$ ).<sup>[9]</sup> These channel structures are pressed against the substrate and filled with protein solutions by capillary forces. Using laminar flow patterns, by means of diffusion gradients of protein solutions can be immobilized. However, this technique is restricted to patterns that can be created by microfluidics.

All the described methods can be classified into direct writing techniques (DPN and spotting) and replication techniques ( $\mu\text{CP}$ ,  $\mu\text{FN}$ ). The first class directly translates digital data to a pattern but is serial in nature. This means that patterning larger areas with higher resolutions will require significantly more time than patterning small areas with low resolution. Replication techniques require a primary replication structure, such as an elastomer stamp, which is translated to a protein pattern. This replication process is parallel in nature so that the processing time is independent of the size and the resolution of the pattern. However, the production of new replication structures to accommodate a modified design may be time-consuming and costly.

If biological responses to a variety of protein patterns are to be examined, techniques are preferable that allow the quick translation of a desired pattern from a digital data set to the usable protein pattern in a short time, without the creation of intermediary components.

In recent years, photolithographic processes have emerged as alternative techniques for the creation of protein patterns. Processing techniques derived from photolithography benefit from decades of research in materials and instrumentation. However, process adaptations need to be implemented to avoid protein damage by high temperatures and UV light. For this purpose “bioresists” have been developed that can be developed and removed using mild conditions under which the protein structure is retained.<sup>[10]</sup> In the fabrication of patterns for cell-based applications toxic compounds need to be omitted, as these compounds may still bleed from the bulk material after curing. Photoinduced radical polymerization of unsaturated compounds such as acrylates is frequently used. With these resists, patterns can be created in analogy to either the classical lift-off process<sup>[11,12]</sup> or a classical etching process.<sup>[13]</sup> Commonly, shadow masks are used, which results in binary patterns. If light is used to activate the surface for protein binding, direct writing techniques permit the formation of grayscale patterns. A number of photochemical approaches have been presented in which covalently bound or adsorbed molecules are activated by illumination. Nitrobenzyl,<sup>[14]</sup> nitroveratryloxycarbonyl,<sup>[15]</sup> and *o*-cinnamoyl groups are commonly used as photocleavable protecting groups, while diazirine,<sup>[16]</sup> phenylazide,<sup>[17]</sup> and benzophenone<sup>[18]</sup> derivatives form highly reactive carbenes, nitrenes, or radicals, respectively, upon irradiation (for reviews, see References [19–21]). The photoreagents are typically coated uniformly onto the substrate and irradiated locally, thus creating a pattern of activated functional groups to which proteins can bind. Related methods make use of the photoinduced coupling of caged ligands to substrate-adsorbed proteins such as bovine serum albumin (BSA).<sup>[22]</sup> The surface-bound protein has to be protected from UV irradiation to avoid denaturation. While photoresists usually only yield binary patterns, photochemical immobilization techniques permit the generation of different gray values and gradients if varying fractions of the caged compounds are activated by irradiation at varying intensities or times.

The so-called “protein adsorption by photobleaching” (PAP) uses photochemical immobilization by means of photobleaching. A fluorescently tagged ligand is incubated on a protein-coated surface (typically BSA). Upon irradiation an oxygen-dependent energy-transfer process transforms the fluorophore into a free-radical species that binds to the protein and thereby immobilizes the attached ligand.<sup>[23]</sup> This coupling strategy has also been used to couple ligands to unsaturated compounds such as methacrylate silanes instead of BSA.<sup>[24]</sup> The main advantage of PAP compared to conventional photochemical or photolithographic techniques is that the fluorophore can be chosen from a wide selection of available dyes, so that the process can be carried out at wavelengths that are not harmful to proteins. Originally this process was proposed by Holden and Cremer using static masks and later a laser beam to create binary patterns.<sup>[23,25]</sup>

Bélisle et al. later proposed modulating the laser intensity to create “grayscale” protein patterns such as density gradients.<sup>[26]</sup> As a serial writing process, laser-assisted PAP suffers from long processing times for larger substrate areas. Therefore, the authors later used bright-field illumination via a light-emitting diode (LED) array through a translucent liquid crystal microdisplay for the generation of light intensity patterns.<sup>[27]</sup> These types of display, generally referred to as spatial light modulators (SLMs), can be used to create a structured pattern of light which is defined by digital data. This technique was shown to be also suitable for the creation of protein gradient patterns on an area of 150 to 200  $\mu\text{m}^2$ . Compared to laser writing, the time required for the generation of a pattern could thus be decreased from 80 to  $\approx 5$  min.<sup>[27]</sup> While this represents a significant increase in processing speed, the method is still too slow to be useful to generate sets of different patterns in a  $\text{cm}^2$  scale area.

Herein, we present a PAP technique using a reflective digital mirror device (DMD; **Figure 1a**). These devices comprise thousands of individually addressable micro mirrors which can be tilted to an on- or off-state, in which incident light is reflected towards the projection plane or to a light dump, respectively. Rapid changes between these states lead to “gray values” of intermediate light intensity by means of pulse width modulation. By setting individual micro-mirror pixels

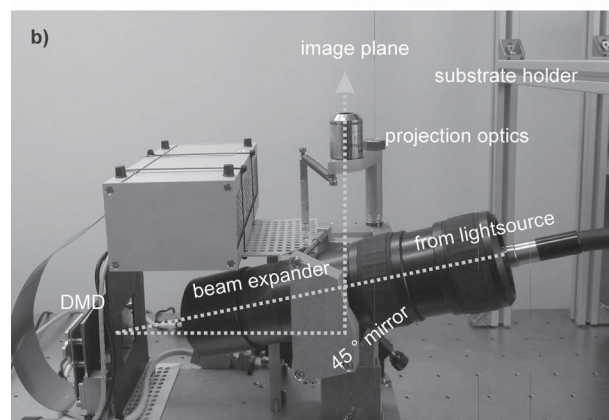
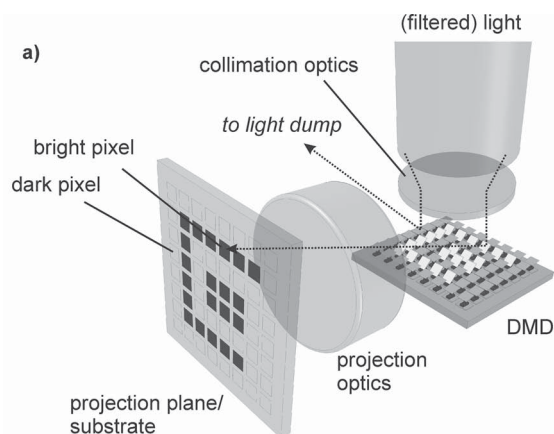


**Figure 1.** a) Basic setup of the lithographic system used in this work. b) Setup of the DMD shown with optical path. The substrate holder on the right is placed above the projection optics to project the image onto the substrate.

to different gray values, light patterns can be created which can be used for various lithographic processes including PAP. The advantage of this reflection-based system compared to translucent SLMs is that it does not suffer from attenuation caused by the light passing through a SLM. Therefore, the overall light intensity is higher and the accessible wavelength range is wider than for SLMs. DMDs are commonly used in projectors and their use for maskless projection lithography has been described.<sup>[28,29]</sup> However, most commercially available DMDs for projector systems can only be used with light sources of limited power to avoid overheating and thus clamping of the micro mirrors. Specific types of DMDs that remain functional when used with strong light sources have to be used for lithographic systems. However, for this type of DMD, the optical setup as well as the control software usually need to be implemented by the user as the DMDs are purchased “as is” with no additional component besides the chip and a digital dynamically linked library (DLL) for software control. Such DMDs have been used to create protein patterns, for example, by deprotection of surface-bound thiol groups that were subsequently conjugated with biotin or proteins.<sup>[30]</sup> However, the authors used the DMD without adding projection optics and thus only patterns with low pixel resolution (in the range of several tens of micrometers) could be obtained. Furthermore, this DMD only allowed the creation of binary patterns.

Herein, we describe a DMD-based lithography system coupled to a high-pressure mercury lamp and equipped with a custom-made demagnifying projection optics which was designed and set up explicitly for high-speed grayscale protein patterning directly from grayscale computerized images by means of PAP.

## 2. Results and Discussion

### 2.1. Lithography System

The lithography system is based on a commercially available DMD with  $1024 \times 768$  individually addressable pixels with a pitch of  $14 \mu\text{m}$ . All parts were custom designed and manufactured in house; optical components as well as the DMD were purchased. The light source used is a superpressure mercury lamp, for our application filtered to  $490 \text{ nm}$  ( $\pm 20 \text{ nm}$ ). In the on-state of each pixel the light is reflected to the projection optics, a fivefold demagnification microscope objective resulting in a projected pixel size of  $2.5 \mu\text{m}$  edge length. The DMD is addressed by means of custom-written software which parses 8-bit grayscale digital bitmap images

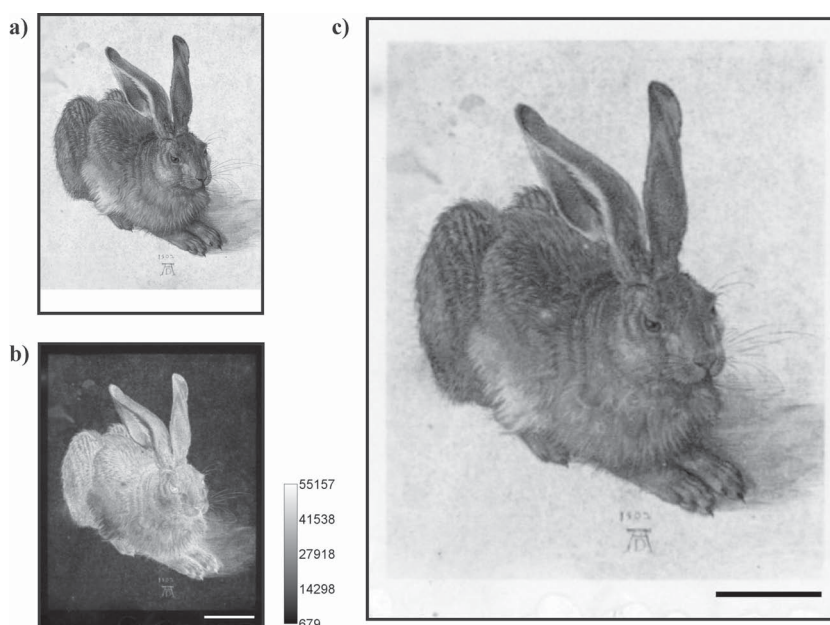


**Figure 2.** Illustration of image quality obtained by the maskless DMD-based lithography system. a) Original image. (Source: [http://en.wikipedia.org/wiki/File:Duerer\\_a\\_young\\_hare.jpg](http://en.wikipedia.org/wiki/File:Duerer_a_young_hare.jpg). Last accessed: March 2012.) b) Pattern of F5B after 10 s of exposure and staining with streptavidin-Cy3 (fluorescence image taken with a photomultiplier gain of 700). c) Inverted image of (b). Frames indicate the outline of the images in the case of the original image and the fluorescence image to indicate exposed and nonilluminated sample areas and background. Scale bar:  $500 \mu\text{m}$ .

as obtained by any image processing software. This image is projected onto an area of about  $2.0 \times 2.7 \text{ mm}^2$  on the substrate. A scheme of the working principle of the DMD system with the optical parts is depicted in Figure 1a, and the setup of the protein pattern generator is shown in Figure 1b.

As a robust and widely known method, covalent coupling of biotin–fluorescein (F5B) to a BSA-coated glass surface and its visualization by binding of fluorescently labeled streptavidin<sup>[23]</sup> was chosen for pattern generation. This way the performance of the maskless DMD could be compared to photopatterning techniques reported in the literature.

The protein pattern generator combined with the BSA–F5B method allows rapid creation of fluorescent streptavidin patterns derived from grayscale bitmaps. To demonstrate the patterning performance, an 8-bit template of “A Young Hare” by Albrecht Dürer exhibiting a variety of gray values and small substructures (Figure 2a) was reproduced as a fluorescent pattern after 10 s of exposure using BSA-coated glass and F5B and subsequent incubation with Cy3-labeled streptavidin (Figure 2b). The inverted image of the fluorescent picture shows that the dynamic range and fine structures are well reproduced (Figure 2c). Note that the bottom of Figure 2a was assigned a gray value brightness of zero and its fluorescence intensity in the reproduced image is equivalent to the nonilluminated background.

### 2.2. Resolution and Dynamic Range

To systematically study the resolution and dynamic range of this DMD-based lithography method, we developed a

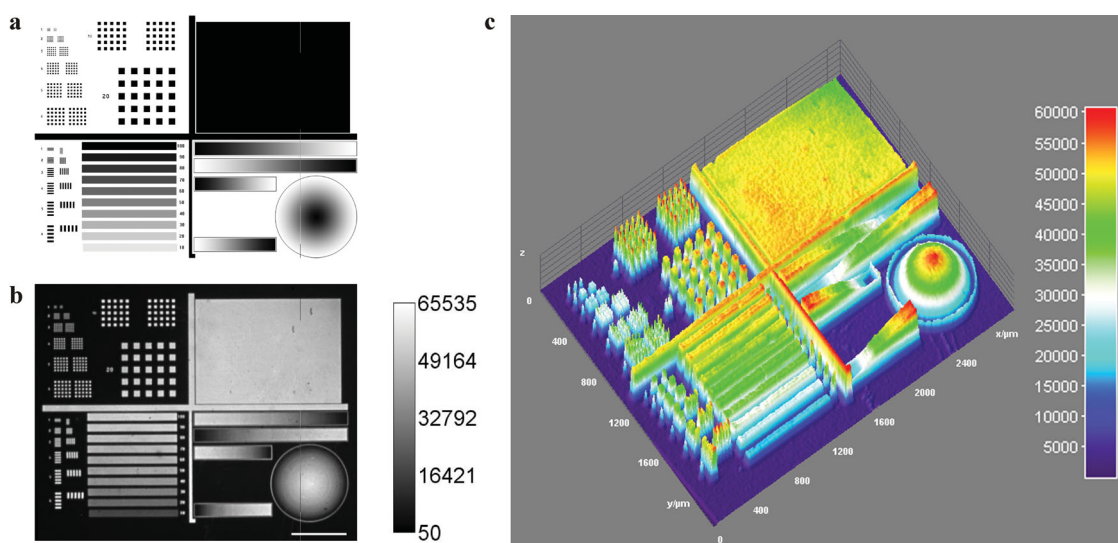


**Figure 3.** Test pattern and visualization of its reproduction by maskless DMD-based lithography. a) Original bitmap (inverted image was used for pattern generation). b) Fluorescence image of streptavidin–Cy3-stained pattern, exposure time 1 min. Scale bar: 500  $\mu\text{m}$ . The fluorescence signal (arbitrary units, see scale bar) is color coded as grayscale values (16 bit). c) Color-coded projection of fluorescence intensity values derived from (b). Color scale shows pixel intensities (a.u.).

test pattern (Figure 3a) that was projected and fluorescently stained for detection. Differences in intensities derived from fluorescence staining (Figure 3b) were examined in a color-coded three-dimensional projection (Figure 3c). The plot shows a steady increase of signal intensity for the one- and two-dimensional gradients (Figure 3c, lower right section) as well as consistent signal intensity for areas exposed with different, uniform intensities (Figure 3c, lower left section; see also Figure 4a,b). A slight increase in intensity can be seen in the upper right corner of the plane and along the cross dividing the image into four quadrants. This is due to slight misalignments or tilting of the substrate to be illuminated in the image plane. This issue will be resolved by changing the way the substrates are fixed on the image plane. However, the error is not systematic in nature (see, e.g., the pixel-by-pixel subtraction of the images displayed in Figure S2, Supporting Information). With the current setup and a fivefold demagnification the projection of one DMD pixel should have an edge length of  $\approx 2.5 \mu\text{m}$ . According to the Abbe equation  $d_{\text{min}} = 1.22\lambda/2 \times \text{NA}$ , the smallest pixel size that can theoretically be resolved with the numerical aperture (NA) of the currently used lens at a wavelength of 490 nm is 2  $\mu\text{m}$ . Therefore, patterns with single-pixel widths or spacings should be recognizable on the substrate.

The resolution of the DMD lithography setup was tested with a pattern of parallel lines with varying widths and spacings (Figure 5a). Lines with a width of only one pixel could be well reproduced (e.g. line around circular gradient, lower right quarter of Figure 3c). Also, lines with a distance and width of one DMD pixel could be clearly resolved by a fluorescence microscope (Figure 5b). The distance of two maxima in Figure 5b is about 5  $\mu\text{m}$ . This number represents the distance between the centers of two one-pixel-wide lines with a one pixel distance so that the effective width of one pixel in the image amounts to about 2.5  $\mu\text{m}$ , which corresponds to the calculated projection size of a DMD pixel.

To reach a pixel size in the submicrometer scale, DMDs with smaller pixels or a lens with a higher demagnification can be used. However, to be able to resolve these features according to Abbe's equation, a lens with a correspondingly higher numerical aperture is needed.

To test the effects of different reflection levels, that is, grayscale values, of the mirrors on F5B immobilization, areas homogeneously exposed to different nominal pixel brightness were investigated (Figure 4a,b). Plotting fluorescence intensity against pixel brightness for a streptavidin–Cy3-stained sample shows a saturation behavior for higher pixel brightnesses (Figure 4b). Likewise, continuous gradients (Figure 4c) show an increasing intensity signal for linearly increasing pixel intensity values with a slight saturation towards higher intensity values (Figure 4d). We assume that depletion of fluorophores in regions with intense irradiation is responsible for the saturation effects seen for high intensity values, as has been previously suggested.<sup>[24]</sup>

In this study, fluorescence intensity values are taken as a measure for the amount of bound streptavidin, as is common practice in protein immobilization.<sup>[15,21,22,24,26]</sup> As described in the literature, protein density has been quantified using dried fluorescently labeled proteins and radioactively labeled proteins, thereby demonstrating that fluorescence intensity can indeed be taken as a measure of protein loading.<sup>[22,31]</sup> It is assumed that due to the relatively short illumination times (10 s to 4 min), the maximum protein loading is not reached in our experiments so that self-quenching of the fluorophores due to spatial proximity can be neglected.

Other methods that are commonly used for the quantification of surface-bound protein, such as X-ray photoelectron spectroscopy (XPS)<sup>[32]</sup> and time-of-flight secondary-ion mass spectrometry (TOF-SIMS),<sup>[13]</sup> are challenging to apply to PAP-patterned surfaces as the immobilized protein is hard to discriminate from the BSA-coated background. The flexibility of the setup allows the creation of any grayscale patterns or gradients that would require tremendous efforts

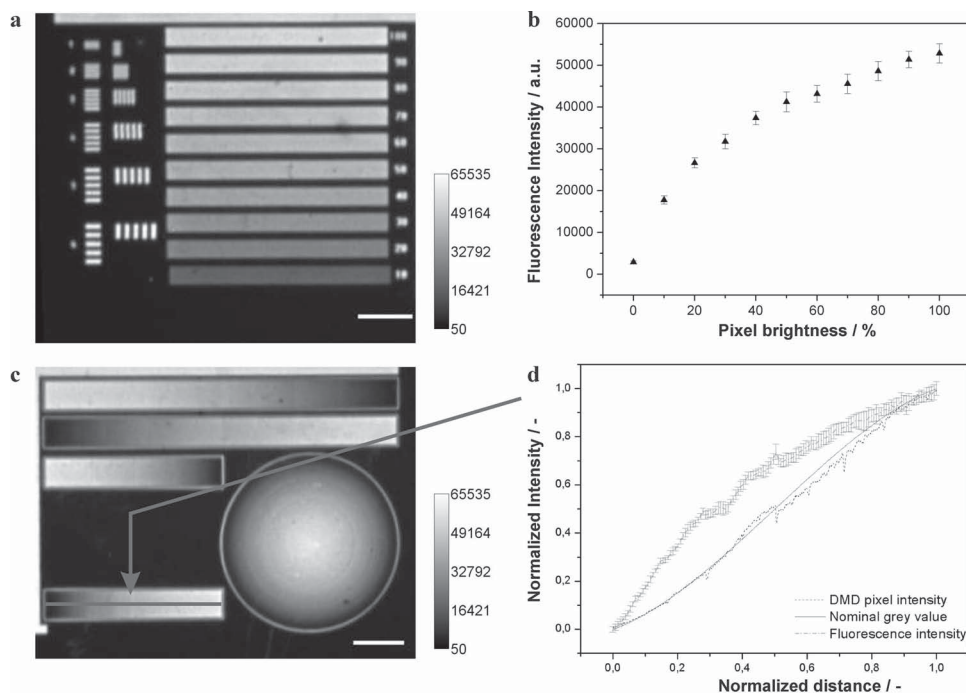


**Figure 4.** Saturation and gradient patterns. a) Fluorescence image of homogeneously exposed areas with pixel brightnesses from 10 to 100%. b) Plot of mean fluorescence intensity versus pixel brightness. 1771 pixels were evaluated per brightness value; standard deviation is indicated by error bars. c) Fluorescence image of continuous gradients. d) Normalized mean intensities of the nominal bitmap gray values compared to measured light intensities on the DMD and fluorescence intensities of a stained sample (intensity ramp marked in (c)). Intensities on the DMD were captured with a video camera through the projection optics (see Figure S1, Supporting Information). For the intensity plot of the DMD signal, 7624 line profiles (each containing 1142 pixels) were evaluated. For the fluorescence signal, 130 line profiles (each containing 18 pixels) were evaluated. Both intensity values and distances along the intensity ramp were normalized. Error bars show standard deviation. Exposure time: 1 min; (a) and (c) are sections of the same sample. Scale bars: 200  $\mu\text{m}$ .

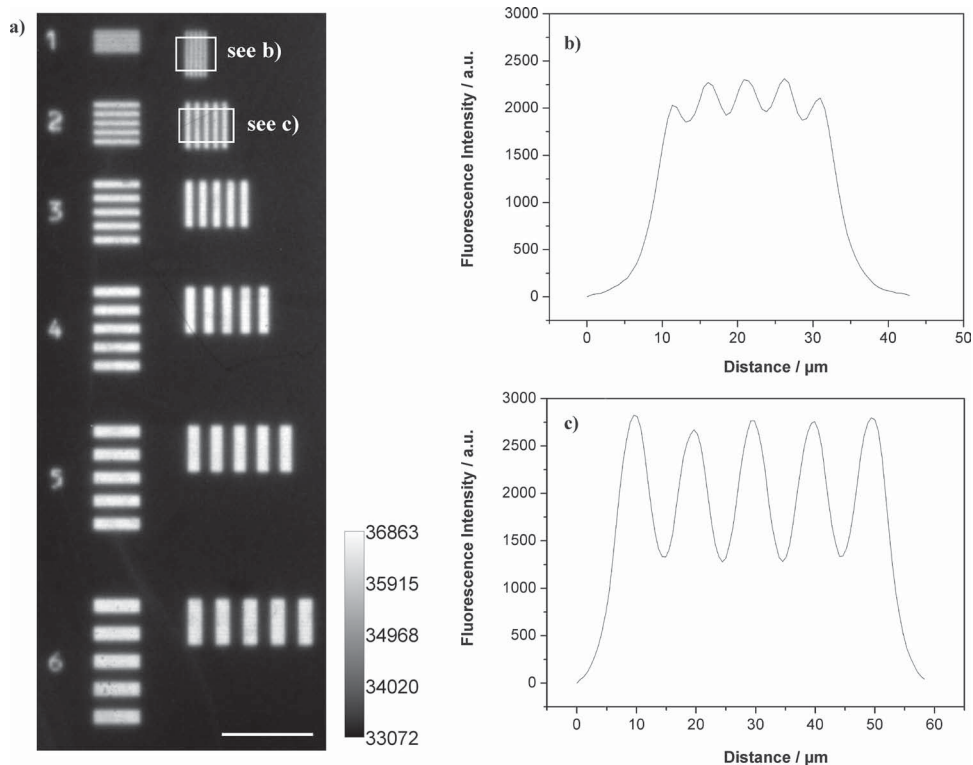


**Figure 5.** Resolution of DMD photolithography. a) Fluorescence image with streptavidin-Cy3-labeled line structures. In every row the line width and line distance are equal and increase from one DMD pixel in the first row to six DMD pixels in the last row, as indicated by numbers. b,c) Mean fluorescence intensity profiles of lines with a width of b) one pixel and c) two pixels (see markers in (a)). Mean fluorescence intensity was calculated out of 60 intensity profiles orthogonal to test lines (area within white boxes). Scale bar: 100  $\mu\text{m}$ .

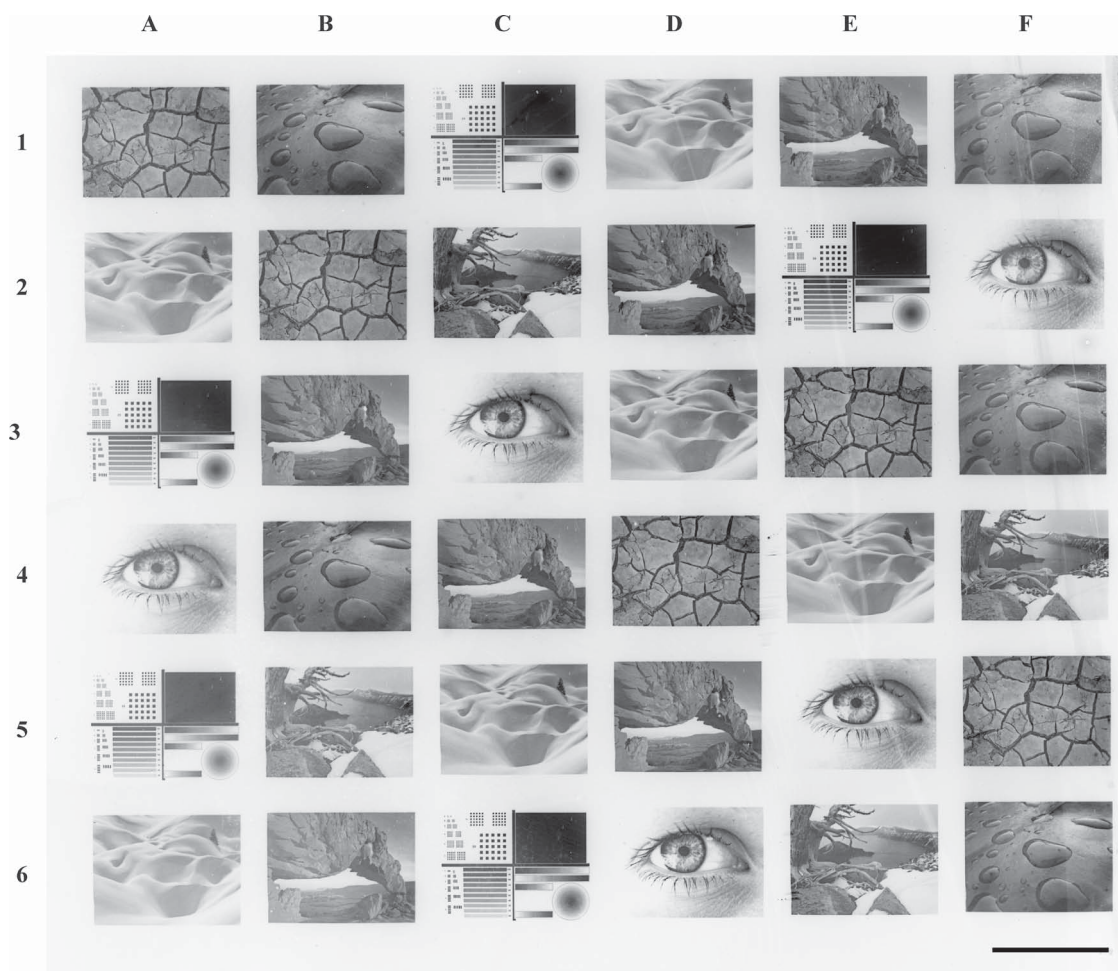


**Figure 6.** Image array illustrating the flexibility of the developed system. Seven different motifs were projected in a random manner. The motifs cover an area of about 2 cm<sup>2</sup> (28.3 million pixels). Exposure time is 1 min per image and 36 min for the whole array. The inverted fluorescence image is shown. Image acquired using a photomultiplier gain of 570; scale bar: 2 mm.

to be obtained by  $\mu$ CP and much longer processing times if produced by any direct writing technique.

The potency and flexibility of the DMD-based approach is demonstrated by an image array (**Figure 6**). The seven chosen grayscale motifs were arranged in a random array that was generated within an overall exposure time of 36 min. The different motifs are recognizable in full detail. Due to staining artifacts, which are mainly caused by inhomogeneous drying of solutions during the staining process, motifs appear in different intensities across the array (compare, e.g., D6 and A4, **Figure 6**) or are disrupted by lines of differing intensity (compare, e.g., columns E, F, **Figure 6**). Such artifacts are known from microarray hybridization. They can be avoided by improved staining procedures or the use of automated hybridization chambers that omit unintended drying of the slides between steps. Calibration patterns across the slide may also help to normalize local protein densities during evaluation.

### 3. Conclusion

The use of a custom-made DMD lithography system as a protein pattern generator eliminates the need for expensive static

masks, which are inflexible and cumbersome to create. DMD-based lithography also allows the rapid exchange of images to be projected within seconds, and is therefore much faster than direct laser writing techniques. As opposed to works presented by Chen and Smith<sup>[30]</sup> in which binary patterns with a resolution of  $>10\ \mu\text{m}$  were obtained with a conventional DMD, the device presented herein allows the creation of grayscale protein patterns and protein gradients with a pixel resolution of about  $2.5\ \mu\text{m}$  in a fast and reproducible manner. Larger areas have been patterned by moving the substrate. As demonstrated, the irradiation time is in the range of 10–60 s per image, which is faster by a factor of 5–30 than with PAP-based systems published in the literature. The current setup allows pixel resolution near the theoretical limit of the optical components.

As this light-activated photobleaching process is wavelength-specific, multiprotein patterns could be created by using fluorophore labels with different absorption wavelengths, as previously shown by others.<sup>[27]</sup> In future work substrate movement will be automated to “stitch” images to gain a multiple of the single image size. This allows the creation of protein patterns of larger lateral size permitting assays to be performed on a larger scale. Such large-scale patterns will also be of interest for the production of functional biomaterials

for diagnostics or implants. Additionally, stronger demagnifying projection optics with appropriate numerical apertures would allow the patterning of even smaller pixels.

Moreover, this system can be used to immobilize proteins using other photochemical reactions, such as the activation of benzophenone or the cleavage of photolabile protecting groups. We believe that such a system is a promising approach for submicrometer multiprotein patterning of areas in the multi-cm<sup>2</sup> range in the near future.

## 4. Experimental Section

**Instrumentation:** For the custom-made lithography system we used a commercially available DMD of type DLP Discovery 4100, purchased from Vialux, Germany. This DMD is designed for lithographic application; it features 1024 × 768 individually addressable pixels (XGA resolution) with a pitch of 14 μm. The mirrors can be set to 256 different gray values via pulse-width modulation. The light intensity measured at the projection plane is linearly related to the increase of white values in the grayscale image set on the DMD. In the projection plane, a light intensity of 10 mW cm<sup>-2</sup> has been measured for a “white image”, which means that all pixels of the DMD are in the on-state. This leads to a computed maximum value of 0.7 nW pixel<sup>-1</sup>. A “black image” corresponds to an overall light intensity of 0 mW cm<sup>-2</sup>. The overall light intensity of a grayscale image can be linearly interpolated and has been experimentally verified (see Figure S3, Supporting Information).

To obtain fast processing speeds we used a strong broad-wavelength light source, a super-pressure mercury lamp (spectrum 280–720 nm, purchased from Lumatec, Germany). The light was filtered with a band filter to 490 nm (±20 nm), which was the required wavelength for the described photobleaching process. The filtered light was passed through a beam-expanding collimation optics (type BE05-10, purchased from Thorlabs, Germany) to illuminate the whole area of the DMD homogeneously. Depending on the setting of each pixel, the light was either deviated to the light dump or to the demagnifying projection optics.

The whole assembly was designed in 3D computer-aided design (CAD) resulting in a construction comprising more than 20 individual components which were manufactured in aluminum by the machine shop in-house. The DMD was addressed by means of custom-written software implemented in the C# programming language. The software uses the dongle-protected library shipped with the DMD. The designed software framework comprises more than 150 000 lines of code and allows the direct parsing of 8-bit grayscale digital bitmap images, which can be created by any image processing software. This image is projected onto the substrate via a 90° reflecting mirror and a demagnification lens which is a fivefold demagnification microscope objective (type MUE10050 LU Plan Fluor EPI 5X, purchased from Nikon, Japan).

Images projected onto the projection plane were recorded with a CMOS USB camera with a resolution of 2048 × 1536 pixels (type Edmund Optics EO-3112C, purchased from Edmund Optics, USA).

Light intensities were measured with bolometers type PowerMax-USB PM30, purchased from Coherent, Germany, and an Intensity Meter 1000, purchased from Karl Süß, Germany.

**Surface Preparation and Lithography:** Surface preparation methods and reagents were used as described elsewhere.<sup>[25]</sup>

Briefly, glass slides (Mentzel, Germany) were coated by immersion in a 3% solution of BSA in phosphate-buffered saline (PBS) for 10 min. After washing three times with PBS, slides were immersed in distilled water and dried by centrifugation. For the picture array (Figure 6) the glass slides were prewashed prior to coating, using a sequence of a solution of ammonia (25%, Merck, Germany), hydrogen peroxide (H<sub>2</sub>O<sub>2</sub>, 35%, Merck, Germany), and distilled water (1:1:5) at 90 °C for 1 h, and a solution of H<sub>2</sub>SO<sub>4</sub> (96%, Merck, Germany), H<sub>2</sub>O<sub>2</sub> (35%), and distilled water (1:1:5) at 90 °C for 1 h. Clean substrates were rinsed with distilled water, dried under nitrogen, and coated as described above.

For lithography a solution of fluorescein-5-biotin (F5B, 80 μM; Sigma–Aldrich, Germany) in PBS was applied to coated slides using a sealed HybriWell chamber (Grace Bio-Labs, USA) and exposed to the image generated by the DMD at 490 nm (±20 nm). After exposure samples were washed three times in PBS and distilled water. To visualize the patterns the slides were incubated for 30 min in a 1:200 diluted solution of streptavidin–Cy3 conjugate (Sigma–Aldrich, Germany) in PBS. After subsequent washing with PBS and distilled water, samples were dried by centrifugation and stored in the dark.

**Fluorescence Measurement:** Fluorescence readout was performed with a GenePix 4000B Microarray Scanner (Molecular Devices, USA) and GenePix software version 6.1. If not stated otherwise, the following settings were used: photomultiplier (PMT) 600, 5 μm resolution per pixel, line average 3, laser power 100%. Resolution was determined by fluorescence microscopy with an IX81-ZDL instrument (Olympus, Japan) equipped with a Hamamatsu C8484-056 CCD camera (Hamamatsu, Japan) using a 10x objective (NA = 0.30) and Olympus CellR 2.1.0.15 software. For intensity measurements and image processing, ImageJ version 1.45a was used.

## Supporting Information

Supporting Information is available from the Wiley Online Library or from the author.

## Acknowledgements

This work received financial support by the “Concept for the Future” of Karlsruhe Institute of Technology (KIT) within the framework of the German Excellence Initiative (Research Group 26-2 and Young Investigator Group 03-109), a Max-Buchner Research fellowship (DECHEMA, MBFSt #2676), as well as a start-up grant by the Young Investigator Network (YIN) of KIT.

- [1] A. Bruckbauer, D. Zhou, L. Ying, Y. E. Korchev, C. Abell, D. Klenerman, *J. Am. Chem. Soc.* **2003**, *125*, 9834–9839.
- [2] R. D. Piner, J. Zhu, F. Xu, S. Hong, C. A. Mirkin, *Science* **1999**, *283*, 661–663.
- [3] J.-H. Lim, D. S. Ginger, K.-B. Lee, J. Heo, J.-M. Nam, C. A. Mirkin, *Angew. Chem.* **2003**, *115*, 2411–2414.

- [4] G. Y. Liu, N. A. Amro, *Proc. Natl. Acad. Sci. USA* **2002**, *99*, 5165–5170.
- [5] R. S. Kane, S. Takayama, E. Ostuni, D. E. Ingber, G. M. Whitesides, *Biomaterials* **1999**, *20*, 2363–2376.
- [6] S. R. Coyer, A. J. García, E. Delamarche, *Angew. Chem. Int. Ed.* **2007**, *46*, 6837–6840.
- [7] M. Mayer, J. Yang, I. Gitlin, D. H. Gracias, G. M. Whitesides, *Proteomics* **2004**, *4*, 2366–2376.
- [8] T. Kraus, R. Stutz, T. E. Balmer, H. Schmid, L. Malaquin, N. D. Spencer, H. Wolf, *Langmuir* **2005**, *21*, 7796–7804.
- [9] E. Delamarche, A. Bernard, H. Schmid, B. Michel, H. Biebuyck, *Science* **1997**, *276*, 779–781.
- [10] W. He, C. R. Halberstadt, K. E. Gonsalves, *Biomaterials* **2004**, *25*, 2055–2063.
- [11] A. Douvas, P. Argitis, K. Misiakos, D. Dimotikali, P. S. Petrou, S. E. Kakabakos, *Biosens. Bioelectron.* **2002**, *17*, 269–278.
- [12] C. D. Diakoumakos, A. Douvas, I. Raptis, S. Kakabakos, D. Dimotikalli, G. Terzoudi, P. Argitis, *Microelectron. Eng.* **2002**, *61–62*, 819–827.
- [13] M. Dubey, K. Emoto, F. Cheng, L. J. Gamble, H. Takahashi, D. W. Grainger, D. G. Castner, *Surf. Interface Anal.* **2009**, *41*, 645–652.
- [14] J. Doh, D. J. Irvine, *J. Am. Chem. Soc.* **2004**, *126*, 9170–9171.
- [15] M. Álvarez, A. Best, S. Pradhan-Kadam, K. Koynov, U. Jonas, M. Kreiter, *Adv. Mater.* **2008**, *20*, 4563–4567.
- [16] Y. Chevolut, O. Bucher, D. Leonard, H. J. Mathieu, H. Sigrüst, *Bioconjugate Chem.* **1999**, *10*, 169–175.
- [17] T. Matsuda, T. Sugawara, *J. Biomed. Mater. Res.* **1995**, *29*, 749–756.
- [18] J. F. Clemence, J. P. Ranieri, P. Aebischer, H. Sigrüst, *Bioconjugate Chem.* **1995**, *6*, 411–417.
- [19] G. Dorman, G. D. Prestwich, *Trends Biotechnol.* **2000**, *18*, 64–77.
- [20] M. Farsari, M. Vamvakaki, B. N. Chichkov, *J. Optics* **2010**, *12*, 124001.
- [21] C. R. Toh, T. A. Fraterman, D. A. Walker, R. C. Bailey, *Langmuir* **2009**, *25*, 8894–8898.
- [22] A. S. Blawas, T. F. Oliver, M. C. Pirrung, W. M. Reichert, *Langmuir* **1998**, *14*, 4243–4250.
- [23] M. A. Holden, P. S. Cremer, *J. Am. Chem. Soc.* **2003**, *125*, 8074–8075.
- [24] J. Scrimgeour, V. K. Kodali, D. T. Kovari, J. E. Curtis, *J. Phys.: Condens. Matter* **2010**, *22*, 194103.
- [25] M. A. Holden, S. Y. Jung, P. S. Cremer, *Anal. Chem.* **2004**, *76*, 1838–1843.
- [26] J. M. Bélisle, J. P. Correia, P. W. Wiseman, T. E. Kennedy, S. Costantino, *Lab Chip* **2008**, *8*, 2164–2167.
- [27] J. M. Bélisle, D. Kunik, S. Costantino, *Lab Chip* **2009**, *9*, 3580–3585.
- [28] S. W. Zhao, H. L. Cong, T. R. Pan, *Lab Chip* **2009**, *9*, 1128–1132.
- [29] D. Kattippambal Rajan, J. Lekkala, *Procedia Eng.* **2010**, *5*, 331–334.
- [30] L. M. Smith, S. Y. Chen, *Langmuir* **2009**, *25*, 12275–12282.
- [31] T. A. Martin, S. R. Caliri, P. D. Williford, B. A. Harley, R. C. Bailey, *Biomaterials* **2011**, *32*, 3949–3957.
- [32] H. Nakayama, J. Nakanishi, T. Shimizu, Y. Yoshino, H. Iwai, S. Kaneko, Y. Horiike, K. Yamaguchi, *Colloids Surf. B* **2010**, *76*, 88–97.
- [33] A. Ivanisevic, M. A. Kramer, H. Jaganathan, *J. Am. Chem. Soc.* **2010**, *132*, 4532–4533.
- [34] M. Pla-Roca, J. G. Fernandez, C. A. Mills, E. Martinez, J. Samitier, *Langmuir* **2007**, *23*, 8614–8618.
- [35] G. M. Whitesides, M. Mayer, J. Yang, I. Gitlin, D. H. Gracias, *Proteomics* **2004**, *4*, 2366–2376.
- [36] C. Padeste, H. Sorribas, L. Tiefenauer, *Biomaterials* **2002**, *23*, 893–900.
- [37] T. Ito, X. Yao, D. A. Higgins, *Langmuir* **2008**, *24*, 8939–8943.
- [38] G. J. Leggett, S. A. A. Ahmad, L. S. Wong, E. ul-Haq, J. K. Hobbs, J. Micklefield, *J. Am. Chem. Soc.* **2011**, *133*, 2749–2759.
- [39] S. B. Petersen, A. K. di enarro, M. T. Neves-Petersen, E. Skovsen, A. Parracino, *Appl. Opt.* **2010**, *49*, 5344–5350.
- [40] J. Nakanishi, H. Nakayama, T. Shimizu, Y. Yoshino, H. Iwai, S. Kaneko, Y. Horiike, K. Yamaguchi, *Colloids Surf. B* **2010**, *76*, 88–97.

Received: October 13, 2011  
 Revised: December 19, 2011  
 Published online: